Book Chapter

A Modified Approach for Bending Vibratory Analysis of Thick Functionally Graded Beams

Youssef Boutahar[1], Nadhir Lebaal[1] and David Bassir[2,3]*

[1]Laboratoire Interdisciplinaire Carnot de Bourgogne, Université Bourgogne Franche-Comté (UTBM), CEDEX, 90010 Belfort, France
[2]Laboratoire LMC, Université Bourgogne Franche-Comté (UTBM), UMR-CNRS 5060, CEDEX, 90010 Belfort, France
[3]Centre Borelli, ENS-University of Paris-Saclay, 91190 Gif-sur-Yvette, France

***Corresponding Author:** David Bassir, Centre Borelli, ENS-University of Paris-Saclay, 91190 Gif-sur-Yvette, France

Published **October 07, 2021**

This Book Chapter is a republication of an article published by David Bassir, et al. at Mathematics in June 2021. (Boutahar, Y.; Lebaal, N.; Bassir, D. A Refined Theory for Bending Vibratory Analysis of Thick Functionally Graded Beams. Mathematics 2021, 9, 1422. https://doi.org/10.3390/math9121422)

How to cite this book chapter: Youssef Boutahar, Nadhir Lebaal, David Bassir. A Modified Approach for Bending Vibratory Analysis of Thick Functionally Graded Beams. In: Leonid Shaikhet, editor. Prime Archives in Applied Mathematics: 2nd Edition. Hyderabad, India: Vide Leaf. 2021.

Abstract

A refined beam theory taking a count the thickness-stretching is presented in this research for bending vibratory behaviour analysis of thick functionally graded (FG) beams. In this theory, the number of unknowns is reduced to four instead of five in the other approaches. Transverse displacement is expressed through a hyperbolic function and subdivided into bending, shear, and thickness-stretching components. The number of unknowns is reduced, which involves a decrease in the number of the governing equation. The boundary conditions at the top and bottom FG-beam faces are satisfied without any shear correction factor. According to a distribution law, effective characteristics of FG beam material change continuously in the thickness direction depending on the constituent's volume proportion. Equations of motion are obtained from Hamilton's principle and are solved by assuming the Navier's solution type, for the case of a supported FG beam, transversely loaded. Numerical results obtained are exposed and analysed in detail to verify the validity of the current theory and prove the influence of the material composition, geometry, shear deformation on the vibratory responses of FG beams, and show the impact of normal deformation on these responses which is neglected in most of the beam theories. The obtained results are compared with those predicted by other beam theories. It can be concluded that the present theory is not only accurate but also simple in predicting the bending and free vibration responses of FG-beam.

Keywords

Refined Beam-Theory; Functionally Graded Beam; Thickness Stretching; Composites; Vibration; Frequency response

Introduction

Functionally graded materials (FGMs) are new types of composites obtained by mixing ceramic and metallic constituents [1-4]. Material properties vary continuously through the beam-thickness in function of the mixing proportion. This avoids the stress concentration observed in laminate composites. FGMs are

reserved for specific uses, for example, coatings of thermal barriers for turbine blades, shielding for military applications, automotive, space and aerospace industries, biomedical materials.

In the past decades, researches on functionally graded material (FGM) beams [5–10], plates [11–19] and shells [20–22] have received substantial attention, and an extensive spectrum of beam and plate theories has been introduced based on the classical beam and plate theories, and shear deformation theories of beam and plate.

FGMs are currently in great demand by industries, requiring very specific models to analyse their behaviour and predict their responses. Many researchers have been interested in different FGM structures analyses because of their wide application areas. Both main beam models, the Euler-Bernoulli model (CBT) for thin beams and the Timoshenko model (SDT) for thick beams, were introduced. CBT model ignores the transverse shear deformation effect. It was modified to take into account the shear deformation into consideration, resulting in the SDT model. Nevertheless, this second model requires a shear correction to satisfy the top and bottom beam faces' boundary conditions, which influences the results. The Higher-order SDT aims to eliminate the failure of CBT and the First-order SDT by assuming a higher-order variation through FG beam thickness for transverse displacement without providing any shear correction.

Multiple models with various shear stress shapes have been proposed, for example, the Reddy model [23].Thai and Vo [24] have presented several refined theories of HSDT beams. They have shown that these models are very effective in the static and dynamic studies of FG and laminates beams. Recently, Ebrahimi et al. [25] Analysed thermo-mechanical vibration of temperature-dependent FGM Beams with porosities by using an HSDT. Aydogdu et al. [26] used the Euler Bernoulli model and parabolic and exponential shear functions to examine the bending vibration-responses of a simply supported FG Beams. Ben Oumrane et al. [7] used different beam theories to

investigate an FG thick Timoshenko-beam's static behaviour. A numerical solution for (TBT) and (HSDT) is presented by Simsek [27] using Ritz method. The finite element method and HSDT are used by Rakesh et al. [28] to analyse the bending vibration responses of the thick FG beams. An analytical solution for the cantilevered thick FG beams is provided by Zhong and Yu [29] for various types of mechanical loads. Based on the neutral surface concept, Ould Larbi et al. [30-31] presented an efficient theory to study bending free vibration of thick FG beams. Similarly, a new First order of SDT theory is developed by Bouremana et al. [33], based on the position of the neutral surface for thick FG beams.

The thickness-stretching impact was introduced first in analysing the vibrational behaviour of thick FG plates [33]. Osofero et al. [34] provided an analysis method of buckling in bending of FG sandwich beams, considering thickness-stretching and shear effects. Meradjah et al. [35] also integrated the thickness-stretching effects in a new shear strain theory to analyse the bending vibration of FG beams.

From the literature mentioned above it is evident that there is no published work considered impact of thickness-stretching on mechanical vibration of FG beams of thick FG beams. This problem is not well-investigated and there is a need for further studies. In this work, a refined theory is presented to analyse bending vibration of thick FG-beam, with supported ends and under transverse loading. This theorie provide a constant transverse displacement and higher-order variation of axial displacement through the depth of the beam so that there is no need for any shear correction factors. By superimposing the deflection on the bending, shear and thickness-stretching parts, the governing equations are derived from Hamilton's principle. The equations system obtained is solved by using Navier's solutions. The material characteristics are presumed to change through the beam thickness following the law of dosing. Detailed mathematical formulations are provided, and example results are proposed to show the relevance of the present theory and to verify this accuracy. Our approach presents the advantage of using less variables in comparation to other theories and it

proves also the effects of thickness-stretching and the influences of many parameters such as material index and slenderness ratio on frequency response and stresses. The proposed higher-order normal deformation and shear theory is not only accurate, but also provides an elegant and easy-to-implement approach to simulating the bending and vibration behaviors of thick FG beams.

Theoretical Formulation

Model Definition

Figure 1 shows the proposed model for this study. It is a thick FG-beam with length (L), rectangular cross-section, width (b) and height (h)

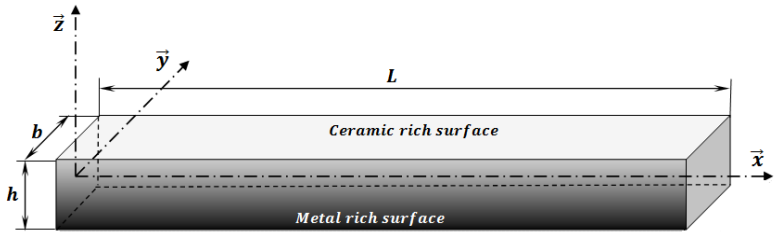

Figure 1: The geometry of the FG-beam

The FG beam is composed of a combination of metal and ceramics whose combination changes from the top surface purely ceramic to the bottom surface completely metallic. The beam material effective characteristic $\mathcal{P}$ is assumed to changes through the FG-beam thickness about the volume ratio and the characteristics of the constituent materials. It is formulated by the law of mixing as follow:

$$\mathcal{P} = \mathcal{P}_m \vartheta_m + \mathcal{P}_c \vartheta_c \ , \ \mathcal{P} = (E, \rho, \nu, \dots \dots) \tag{1}$$

E, ρ, ν are Young modulus, mass density and Poisson's coefficient, respectively. Variation of ν is generally small, so it remains constant.$\vartheta_c$and $\vartheta_m$are ceramic and metal volume proportions respectively, defined by [36]:

$$\vartheta_m + \vartheta_c = 1, \quad \vartheta_c = \left(0.5 + {}^{z}/_{h}\right)^{p}, \qquad p \geq 0 \tag{2}$$

The gradient index(p), with $p \geq 0$ determines the profile of the material in the FG beam thickness direction. It can be modified to obtain the optimum component materials distribution. The plot in figure 2 shows the distribution of ceramic volume proportion across the FG beam thickness for various material indexes.

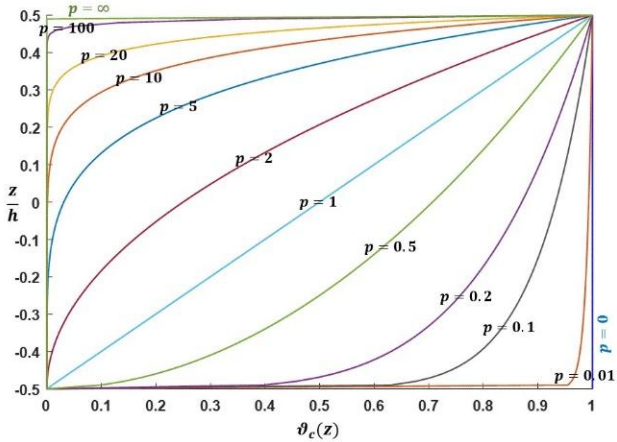

Figure 2: Ceramic volume proportion profile across FG beam thickness, for different material indexes

Each effective characteristic of the FG beam can be expressed as follows:

$$\mathcal{P}(z) = (\mathcal{P}_c - \mathcal{P}_m)\left(0.5 + {}^{z}/_{h}\right)^{p} + \mathcal{P}_m \ , \qquad \mathcal{P} = E, \rho \tag{3}$$

Displacement and Strain Fields

Transverse and axial displacements of the FG-beam are expressed, according to the quasi-3D theory [35,37] as follow:

$$\begin{cases} U(x,z) = u_0(x) - z\,\partial w_b/\partial x - f(z)\,\partial w_s/\partial x \\ W(x,z) = w_b(x) + w_s(x) + w_{st}(x) \end{cases} \tag{4}$$

With,

$$w_{st}(x) = g(z)\phi(x), \quad g(z) = 1 - df(z)/dz \tag{5}$$

u_0 : *Axial displacement*
w_b : *Bending transverse displacement*
w_s : *Shear transverse displacement*
w_{st}: *Thickness-Stretching displacement*
u_0, w_b, w_s *and* ϕ*are four unknowns to be determined*
$f(z)$ *and* $g(z)$ *are the shape functions*

The strains are as follows:

$$\begin{cases} \varepsilon_x = \partial u_0/\partial x - z\,\partial^2 w_b/\partial x^2 - f(z)\,\partial^2 w_s/\partial x^2 \\ \varepsilon_z = (dg(z)/dz)\phi \\ \gamma_{xz} = g(z)[\partial w_s/\partial x + \partial\phi/\partial x] \end{cases} \tag{6}$$

The FG beam material follows Hooke's law. So, linear elastic equation can be expressed as:

$$\begin{Bmatrix} \sigma_x \\ \sigma_z \\ \tau_{xz} \end{Bmatrix} = E(z) \begin{bmatrix} 1 & \nu & 0 \\ \nu & 1 & 0 \\ 0 & 0 & \dfrac{1}{2(1+\nu)} \end{bmatrix} \begin{Bmatrix} \varepsilon_x \\ \varepsilon_z \\ \gamma_{xz} \end{Bmatrix}$$

$$= E(z) \begin{Bmatrix} \dfrac{\partial u_0}{\partial x} - z\dfrac{\partial^2 w_b}{\partial x^2} - f(z)\dfrac{\partial^2 w_s}{\partial x^2} + \nu\dfrac{dg(z)}{dz}\phi \\ \nu\dfrac{\partial u_0}{\partial x} - \nu z\dfrac{\partial^2 w_b}{\partial x^2} - \nu f(z)\dfrac{\partial^2 w_s}{\partial x^2} + \dfrac{dg(z)}{dz}\phi \\ \dfrac{1}{2(1+\nu)}\left(\dfrac{\partial w_b}{\partial x} + \dfrac{\partial w_s}{\partial x}\right) \end{Bmatrix} \tag{7}$$

Calculation of Energies

- Strain energy

$$\begin{cases} \delta\mathcal{U} = \int_0^L \int_0^b \left[\int_{-\frac{h}{2}}^{\frac{h}{2}} (\sigma_x \delta\varepsilon_x + \tau_{xz}\delta\gamma_{xz} + \sigma_z\delta\varepsilon_z) dz \right] dydx \\ = \int_0^L \left(\mathcal{N}_x \frac{\partial \delta u_0}{\partial x} - \mathcal{M}_x^b \frac{\partial^2 \delta w_b}{\partial x^2} - \mathcal{M}_x^s \frac{\partial^2 \delta w_s}{\partial x^2} + \mathcal{Q}_{xz} \left(\frac{\partial \delta w_s}{\partial x} + \frac{\partial \delta\phi}{\partial x} \right) + \mathcal{N}_z \delta\phi \right) dx \end{cases} \tag{8}$$

where, $\mathcal{N}_x$, $\mathcal{M}_x^b$, $\mathcal{M}_x^s$, $\mathcal{Q}_{xz}$and $\mathcal{N}_z$ are the stress resultants, specified as:

$$\begin{cases} (\mathcal{N}_x, \mathcal{M}_x^b, \mathcal{M}_x^s) = \int_{-h/2}^{h/2} [1, z, f(z)]\sigma_x \, bdz \\ \mathcal{Q}_{xz} = \int_{-h/2}^{h/2} \tau_{xz} g(z) b dz \\ \mathcal{N}_z = \int_{-h/2}^{h/2} \sigma_z \frac{dg(z)}{dz} b dz \end{cases} \tag{9}$$

By using equation (7), the stress resultants given in equation (9) can be expressed as:

$$\begin{Bmatrix} \mathcal{N}_x \\ \mathcal{M}_x^b \\ \mathcal{M}_x^s \\ \mathcal{Q}_{xz} \\ \mathcal{N}_z \end{Bmatrix} = \begin{bmatrix} \mathcal{A} & \mathcal{B} & \mathcal{B}_s & \mathcal{X} & 0 \\ \mathcal{B} & \mathcal{D} & \mathcal{D}_s & \mathcal{Y} & 0 \\ \mathcal{B}_s & \mathcal{D}_s & \mathcal{H}_s & \mathcal{Y}_s & 0 \\ \mathcal{X} & \mathcal{Y} & \mathcal{Y}_s & \mathcal{Z} & 0 \\ 0 & 0 & 0 & 0 & \mathcal{A}_s \end{bmatrix} \begin{Bmatrix} \frac{\partial u_0}{\partial x} \\ -\frac{\partial^2 w_b}{\partial x^2} \\ -\frac{\partial^2 w_s}{\partial x^2} \\ \left(\frac{\partial w_s}{\partial x} + \frac{\partial \phi}{\partial x} \right) \end{Bmatrix} \tag{10}$$

$(\mathcal{A}, \mathcal{B}, \mathcal{D}, \mathcal{B}_s, \mathcal{D}_s, \mathcal{H}_s, \mathcal{X}, \mathcal{Y}, \mathcal{Y}_s, \mathcal{Z}, \mathcal{A}_s)$ are the FG-beam stiffness expressed, and are given by the Appendix A.

- Potential energy due the external transverse load applied

$$\delta\mathcal{V} = -\int_0^L q(x)\delta W dx \; = -\int_0^L q(x)\delta(w_b + w_s + w_{st}) dx \tag{11}$$

q(x): External transverse loading.

- Kinetic energy

$$\begin{cases} \delta\mathcal{K} = \int_0^L \int_0^b \left[\int_{-h/2}^{h/2} \rho(z)\left(\dot{U}\delta\dot{U} + \dot{W}\delta\dot{W}\right) dz \right] dydx \\ = \int_0^L \left(I_0[\dot{u}_0\delta\dot{u}_0 + (\dot{w}_b + \dot{w}_s)(\delta\dot{w}_b + \delta\dot{w}_s)] + J_0\left[(\dot{w}_b + \dot{w}_s)\delta\dot{\phi} + \dot{\phi}\delta(\dot{w}_b + \dot{w}_s)\right]\right) dx \\ - \int_0^L \left(I_1\left[\dot{u}_0\frac{\partial\delta\dot{w}_b}{\partial x} + \frac{\partial\dot{w}_b}{\partial x}\delta\dot{u}_0\right] + I_2\frac{\partial\dot{w}_b}{\partial x}\frac{\partial\delta\dot{w}_b}{\partial x} + J_1\left[\dot{u}_0\frac{\partial\delta\dot{w}_s}{\partial x} + \frac{\partial\dot{w}_s}{\partial x}\delta\dot{u}_0\right]\right) dx \\ - \int_0^L \left(K_2\frac{\partial\dot{w}_s}{\partial x}\frac{\partial\delta\dot{w}_s}{\partial x} - J_2\left[\frac{\partial\dot{w}_b}{\partial x}\frac{\partial\delta\dot{w}_s}{\partial x} + \frac{\partial\dot{w}_s}{\partial x}\frac{\partial\delta\dot{w}_b}{\partial x}\right] + K_0\dot{\phi}\delta\dot{\phi}\right) dx \end{cases} \tag{12}$$

where$(I_0, I_1, I_2, J_0, J_1, J_2, K_0, K_2)$are mass inertias, and are given by the Appendix A:

Governing Equation

To obtain the beam governing-equation, the Hamilton principle is applied as follows:

$$\int_{t1}^{t2}(\delta\mathcal{U} + \delta\mathcal{V} - \delta\mathcal{K})\mathrm{dt} = 0 \tag{13}$$

Substituting the expressions for $\delta\mathcal{U}, \delta\mathcal{V}$ and $\delta\mathcal{K}$ from equations (8), (11) and (12) into equation (13), and the following system is obtained by integrating by parts, and bringing together the coefficients of $\delta u_0, \delta w_b, \delta w_s$ and $\delta\phi$.

$$\begin{cases} \delta u_0 : \frac{\partial\mathcal{N}_x}{\partial x} = I_0\ddot{u}_0 - I_1\frac{\partial\ddot{w}_b}{\partial x} - J_1\frac{\partial\ddot{w}_s}{\partial x} \\ \delta w_b : \frac{\partial^2\mathcal{M}_x^b}{\partial x^2} + q = I_0(\ddot{w}_b + \ddot{w}_s) + I_1\frac{\partial\ddot{u}_0}{\partial x} - I_2\frac{\partial^2\ddot{w}_b}{\partial x^2} - J_2\frac{\partial^2\ddot{w}_s}{\partial x^2} + J_0\ddot{\phi} \\ \delta w_s : \frac{\partial^2\mathcal{M}_x^s}{\partial x^2} + \frac{\partial\mathcal{Q}_{xz}}{\partial x} + q = I_0(\ddot{w}_b + \ddot{w}_s) + J_1\frac{\partial\ddot{u}_0}{\partial x} - J_2\frac{\partial^2\ddot{w}_b}{\partial x^2} - K_2\frac{\partial^2\ddot{w}_s}{\partial x^2} + J_0\ddot{\phi} \\ \delta\phi : \frac{\partial\mathcal{Q}_{xz}}{\partial x} - \mathcal{N}_z = J_0(\ddot{w}_b + \ddot{w}_s) + K_0\ddot{\phi} \end{cases} \tag{14}$$

Equation (14) can be expressed in terms of displacement of u_0, w_b, w_s and ϕ by using equation (10) as follows:

$$\begin{cases} \delta u_0: \mathcal{A}\frac{\partial^2 u_0}{\partial x^2} - \mathcal{B}\frac{\partial^3 w_b}{\partial x^3} - \mathcal{B}_s\frac{\partial^3 w_s}{\partial x^4} + \mathcal{X}\frac{\partial \phi}{\partial x} = I_0\ddot{u}_0 - I_1\frac{\partial \ddot{w}_b}{\partial x} - J_1\frac{\partial \ddot{w}_s}{\partial x} \\ \delta w_b: \mathcal{B}\frac{\partial^3 u_0}{\partial x^3} - \mathcal{D}\frac{\partial^4 w_b}{\partial x^4} - \mathcal{D}_s\frac{\partial^4 w_s}{\partial x^4} + \mathcal{Y}\frac{\partial^2 \phi}{\partial x^2} + q = I_1\frac{\partial \ddot{u}_0}{\partial x} + I_0(\ddot{w}_b + \ddot{w}_s) - I_2\frac{\partial^2 \ddot{w}_b}{\partial x^2} - J_2\frac{\partial^2 \ddot{w}_s}{\partial x^2} + J_0\ddot{\phi} \\ \delta w_s: \mathcal{B}_s\frac{\partial^3 u_0}{\partial x^3} - \mathcal{D}_s\frac{\partial^4 w_b}{\partial x^4} - \mathcal{H}_s\frac{\partial^4 w_s}{\partial x^4} + \mathcal{A}_s\frac{\partial^2 w_s}{\partial x^2} + (\mathcal{A}_s + \mathcal{Y}_s)\frac{\partial^2 \phi}{\partial x^2} + q = J_1\frac{\partial \ddot{u}_0}{\partial x} + I_0(\ddot{w}_b + \ddot{w}_s) \\ \quad -J_2\frac{\partial^2 \ddot{w}_b}{\partial x^2} - K_2\frac{\partial^2 \ddot{w}_s}{\partial x^2} + J_0\ddot{\phi} \\ \delta\phi: \mathcal{X}\frac{\partial u_0}{\partial x} - \mathcal{Y}\frac{\partial^2 w_b}{\partial x^2} + (\mathcal{A}_s + \mathcal{Y}_s)\frac{\partial^2 w_s}{\partial x^2} - \mathcal{A}_s\frac{\partial^2 \phi}{\partial x^2} + Z\phi = J_0(\ddot{w}_b + \ddot{w}_s) + K_0\ddot{\phi} \end{cases} \quad (15)$$

Analytical Solution for a Simple Supported Functionally Graded Beam (S-S FG-Beam)

Analytical solutions of the motion equations are provided, based on Navier type solutions. The following displacements u_0, w_b, w_s and $\phi$are assumed to be combinations of known trigonometric functions which satisfy the boundary conditions and unknown coefficients to be determined for each

value of"n". $\begin{bmatrix} u_0(x,t) \\ w_b(x,t) \\ w_s(x,t) \\ \phi(x,t) \end{bmatrix} = \sum_{n=1}^{\infty} \begin{bmatrix} U_n\, cos(\lambda x)e^{i\omega_n t} \\ W_{bn}\, sin(\lambda x)e^{i\omega_n t} \\ W_{sn}\, sin(\lambda x)e^{i\omega_n t} \\ \phi_n\, sin(\lambda x)e^{i\omega_n t} \end{bmatrix}$ (16)

$\omega_n$is the eigenfrequency associated with the n^{th} eigenmode, $\lambda = n\pi/L$, and U_n, W_{bn}, W_{sn} and ϕ_n are the unknown coefficients.

The following boundary conditions are imposed for a beam with two ends simply supported.

$$U = W = \mathcal{M}_x^b = \mathcal{M}_x^s = 0 \quad (17)$$

The assumed mechanical transverse load $q(x)$ is developed in a sinusoidal Fourier series as:

$$q(x) = \sum_{n=1}^{\infty} Q_n \sin(\lambda x) \tag{18}$$

The coefficients Q_n are provided below for some loads.

- *Sinusoidal distribution case:*

$$n = 1 \Longrightarrow Q_1 = q_0 \tag{19}$$

- *Uniform distribution case:*

$$Q_n = \frac{4q_0}{n\pi}, \quad (n = 1, 3, 5) \tag{20}$$

So, analytical solutions may be reached from the eigenvalues system below for any fixed value of "n":

$$([K] - \omega_n^2[M])\{\Delta\} = \{F\} \tag{21}$$

In the static problem case, equation (24) becomes:

$$[K]\{\Delta\} = \{F\} \tag{22}$$

$$[K] = \begin{bmatrix} k_{11} & k_{12} & k_{13} & k_{14} \\ k_{12} & k_{22} & k_{23} & k_{24} \\ k_{13} & k_{11} & k_{33} & k_{34} \\ k_{14} & k_{24} & k_{34} & k_{44} \end{bmatrix}, [M] = \begin{bmatrix} m_{11} & m_{12} & m_{13} & 0 \\ m_{12} & m_{22} & m_{23} & m_{24} \\ m_{13} & m_{23} & m_{33} & m_{34} \\ 0 & m_{24} & m_{34} & m_{44} \end{bmatrix}, \{\Delta\} = \begin{Bmatrix} U_n \\ W_{bn} \\ W_{sn} \\ \phi_n \end{Bmatrix}, \{F\} = \begin{Bmatrix} 0 \\ Q_n \\ Q_n \\ 0 \end{Bmatrix} \tag{23}$$

$(k_{11}, k_{12}, k_{23}, k_{22}, k_{13}, k_{24}, k_{33}, k_{14}, k_{34}, k_{44})$ and $(m_{11}, m_{12}, m_{13}, m_{22}, m_{23}, m_{24}, m_{33}, m_{34}, m_{44})$ are given by the Appendix A

Numerical Results and Discussion

In this part, a uniform transverse load is applied to the S-S FG beam. Numerical examples are proposed first to validate the model presented above and assess its accuracy. The FG-beam

material is composed by Al_2O_3(Alumina) and Al(Aluminium). The material characteristics of the corresponding components are listed in table1.

Table 1: Material characteristics of $Al_2O_3$and Al [38].

Components	$\boldsymbol{\nu}$	$\boldsymbol{E(GPa)}$	$\boldsymbol{\rho\ (kg/m^3)}$
Ceramic **(alumina $\boldsymbol{Al_2O_3}$)**	0.3	380	3960
Metal **(aluminium $\boldsymbol{Al}$)**	0.3	70	2702

The dimensionless form is used as follows:

$$\bar{U} = 100\left(\frac{E_m h^3}{q_0 L^4}\right) U\left(0, -\frac{h}{2}\right); \qquad \bar{W} = 100\left(\frac{E_m h^3}{q_0 L^4}\right) W(L/2, h/2)$$

$$\overline{\sigma_{xz}} = \left(\frac{h}{q_0 L}\right)\sigma_{xz}(0,0); \qquad \bar{\sigma}_z = \left(\frac{h}{q_0 L}\right)\sigma_z\left(\frac{L}{2}, \frac{h}{2}\right); \quad \bar{\omega} = (\omega L^2/h)\sqrt{\frac{\rho_m}{E_m}} \tag{24}$$

A numerical example set out in table 2 is performed for various material indexes to validate the present model. The results obtained by this theory concerning displacements and the stresses for (L/h=5) are compared with those of the analytical solution provided by Li et al. [39]. The following shape function based on Reddy beam theory is used:

$$f(z) = \frac{4z^3}{3h^2} \tag{25}$$

Static Analysis

Table2 reveals that the present theory is with good agreement compared to the results obtained by Li et al. [39] and thus confirm the validation of the proposed method. It can also be seen that the CBT model, which omits shear deformation effects under-estimates displacements and stresses of the thick FG beams.

Table 2: Comparison of Non- dimensional transverse and axial displacements, axial and shear stresses of S-S FG-beam for various material indexes

p	**Theory**	$L/h = 5$			
		$\overline{W}$	$\overline{U}$	$\overline{\sigma}_x$	$\overline{\sigma}_{xz}$
0	Li et al. [39]	3.1657	0.9402	3.8020	0.7500
	CBT	2.8783	0.9211	3.7500	-
	Present	3.1681	0.9406	3.7919	0.7503
0.5	Li et al. [39]	4.8292	1.6603	4.9925	0.7676
	CBT	4.4401	1.6331	4.9206	-
	Present	4.8202	1.6653	4.9893	0.7674
1	Li et al. [39]	6.2599	2.3045	5.8837	0.7500
	CBT	5.7746	2.2722	5.7959	-
	Present	6.2475	2.2903	5.8797	0.7503
5	Li et al. [39]	9.7802	3.7089	8.1030	0.5790
	CBT	8.7508	3.6496	8.1329	-
	Present	9.7787	3.6955	8.1099	0.5867
10	Li et al. [39]	10.8979	3.8860	9.7063	0.6436
	CBT	9.6072	3.8097	9.5228	-
	Present	10.8847	3.8780	9.7086	0.6645

To investigate again the effects of the thickness stretching on displacements, a comparison between the non-dimensional displacements of the beam obtained from the present model with and without thickness stretching is made in Figures 3.a and 3.b for the transverse and axial displacements, respectively, for (L/h=5) and (p=5). The difference between the two curves is seen. It is large out in the middle of the beam and becomes zero at the ends for the transverse displacement and becomes zero out in the middle of the beam for the axial displacement, unlike for the axial displacement, which is large at the ends and vanishes out in the middle of the beam.

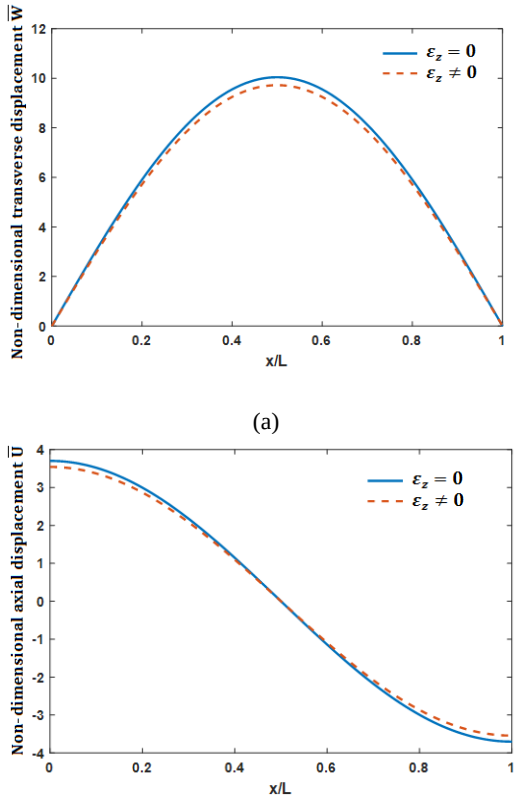

Figure 3: Thickness stretching effect on the non-dimensional transverse and axial displacements.

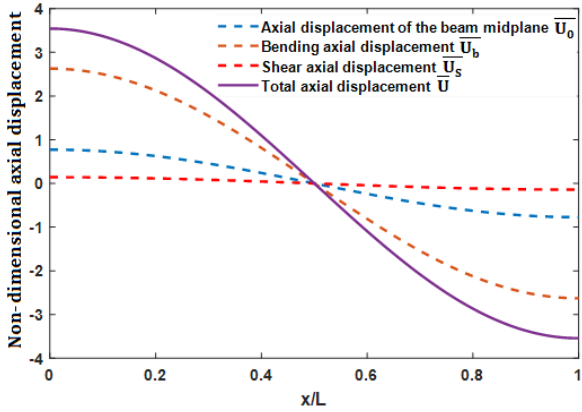

(a)

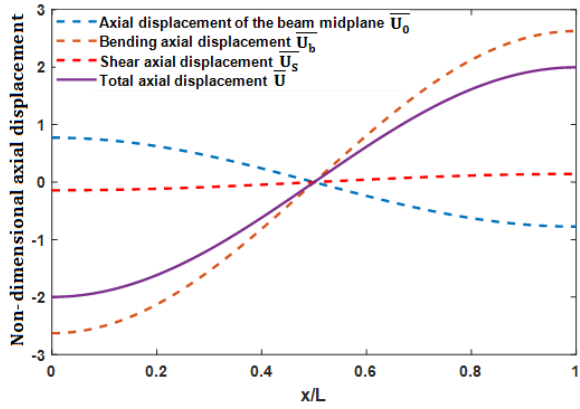

(b)

Figure 4: Shear effect on axial displacement a long of the FGB on (a) Lower beam face and (b) Upper beam face.

Effect of shear on the evolution of non-dimensional axial displacement along the beam on the upper and lower beam faces is evaluated from figure 4, for (L/h=5) and (p=5). We notice that shear have a very slight effect on the axial displacement. It can also be seen that shear is maximum at the ends and zero at the mid-span of the beam.

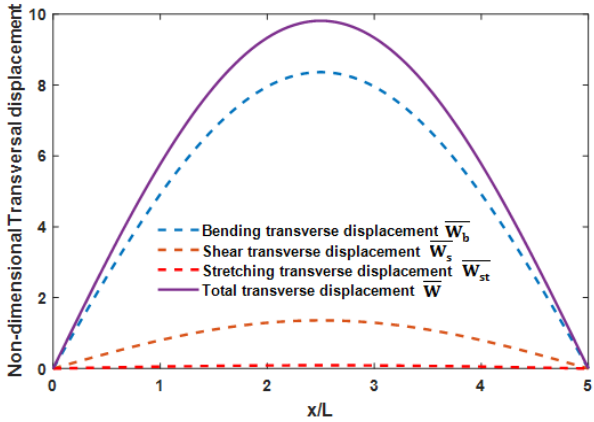

Figure 5: Shear and stretching effects on (a) axial displacement and (b) transverse displacement.

In the second examination and analysis example, effects of shear and thickness stretching on the non-dimensional axial and transverse displacements of the S-S FG-beam are evaluated in figure 5, for (L/h=5) and (p=5). It is obvious from these figures that the shear effect is more important on the two displacements, and it is greatest than the effect of thickness stretching for the transverse displacement. So, the shear effect on the displacements cannot be neglected, especially for the thick beams.

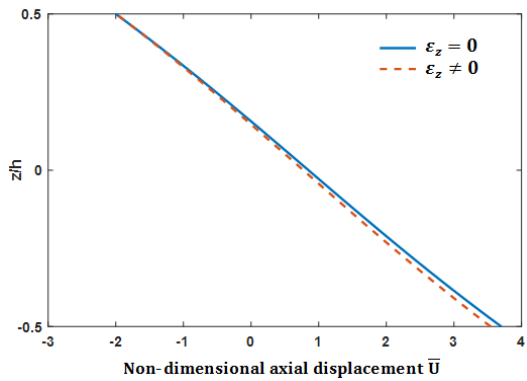

(a)

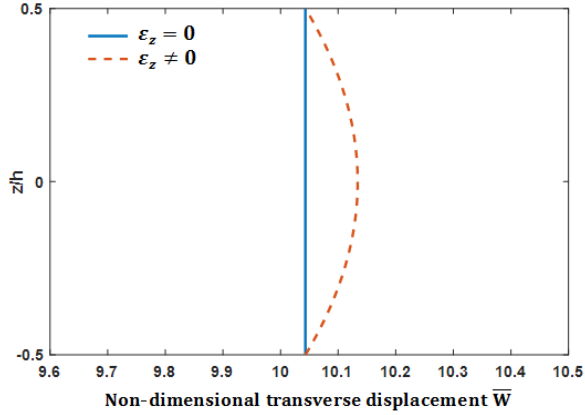

(b)

Figure 6: Non-dimensional: (a) Axial displacement$\overline{U}$, (b) Mid-span deflection $\overline{W}$ through the FG-beam thickness.

In figures 6.a and 6.b, the evolution of non-dimensional (a) in-plane displacement at the end $\overline{U}(0)$ and (b) transverse displacement $\overline{W}(L/2)$ at mid-span through the FG beam thickness under uniform load is presented for (L/h=5) and (p=5). A slight difference appears for this shortest beam. It is seen that the maximum displacement is at the bottom of the beam for axial displacement and the median plane for transverse displacement. This is due to the consideration of the thickness stretching ($\varepsilon_z \neq 0$).

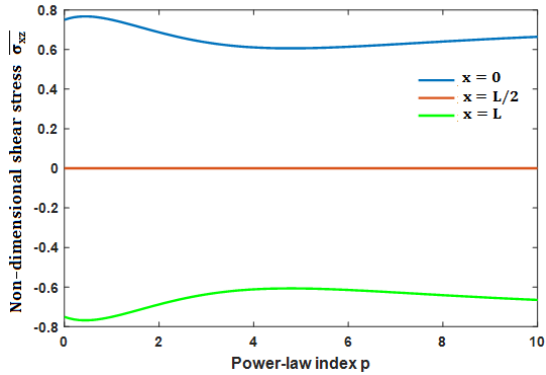

(a)

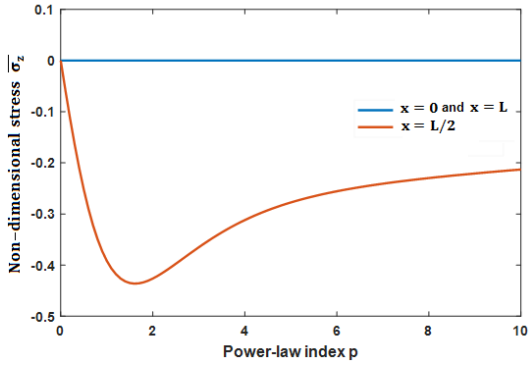

(b)

Figure 7: Non-dimensional: (a) Shear stress$\overline{\sigma_{xz}}$, (b) stress due to the thickness stretching$\overline{\sigma_z}$ versus the material parameter.

Figures 7.a and 7.b illustrate the evolution of the non-dimensional (a) transverse shear stress, (b) stress due to the thickness stretching, versus power-law index$(p)$for (L/h=5). All curves display the material index dependence of the stresses. It is clear that stress due to the thickness stretching exhibit low values but not negligible compared with those of the transverse shear stress.

Variations of the non-dimensional axial stress$\overline{\sigma_x}$across the depth and versus non-dimensional length of the FGB are presented in figures 8.a and 8.b for (L/h=5) and (p=5). The axial stress is zero at the end edges, but it is maximum at the middle of the beam, and The upper beam face is stretched. On the other hand, the lower face is compressed. Extension stress at the upper beam face is higher than the compressive stress at the lower face because at the upper face, the beam is ceramic-rich, whereas, at the lower face, it is metal-rich. It is observed that the neutral plan with zero axial stress is moved upwards relative to the middle position. This is due to the non-homogeneous material of the FG-beam (p=5).

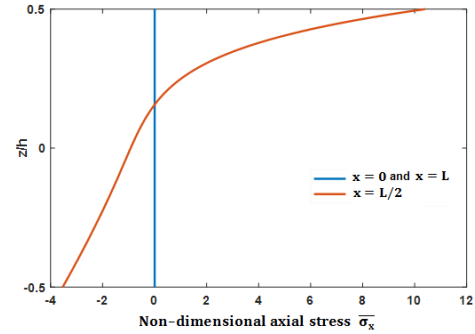

(a)

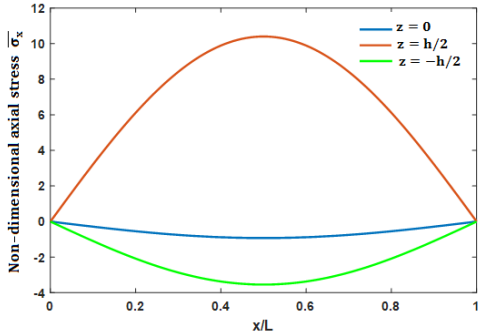

(b)

Figure 8: $\overline{\sigma_x}$distributions: (a) over the FG-beam thickness, (b) versus the FG-beam non-dimensional length

In figures 9.a and 9.b are plotted the distributions of the non-dimensional shear stress$\overline{\sigma_{xz}}$through thethickness and versus non-dimensional length of the FG beam, respectively, for (L/h=5) and (p=5). These figures reveal that the shear stress reaches its maximum value at the beam ends but with opposite signs. It is cancelled in the middle of the beam on the neutral plane and the lower and upper faces. As a result, the conditions of non-shearing on both lower and upper faces of the beam are satisfied.

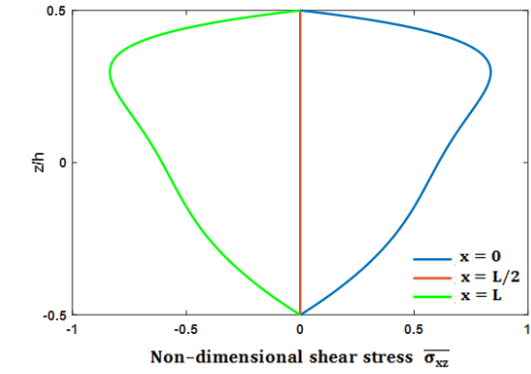

(a)

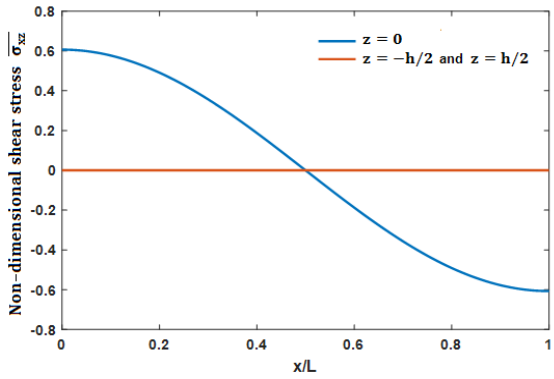

(b)

Figure 9: $\overline{\sigma_{xz}}$ distributions: (a) over the FG-beam thickness, (b) versus the FG-beam non-dimensional length

Thickness-stretching impact on the stresses is evaluated in figures 10.a and 10.b for (L/h=5) and (p=5). It may be seen that$\overline{\sigma_z}$is equal to zero at both end edges. Its highest value is reached in the middle of the beam. The upper beam face is stretched. On the other hand, the lower face is compressed. Compressive stress at the FG beam's lower face is higher than extension stress at the upper face.

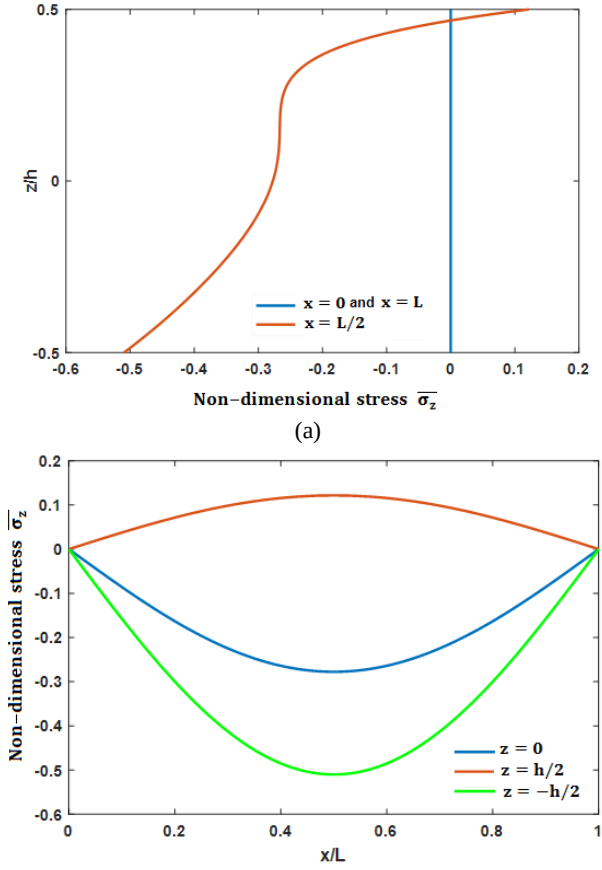

Figure 10: $\overline{\sigma_z}$ distributions: (a) over the FG-beam thickness, (b) versus the FG-beam non-dimensional length

Dynamic Analysis

Table 4 summarises dimensionless frequencies associated with the first, second and third mode shapes of the S-S FG-beam for various (L/h) ratio and material parameter (p).

Table 3: Comparison of the S-S FG-beam frequencies$\overline{\omega_i}$ for some values of (L/h) and (p).

L/h	Mode	Theory		p				
				0	0.5	1	5	10
5	1	HSDT [30]	$\varepsilon_z = 0$	5.1530	4.4110	3.9900	3.4000	3.2810
		Present	$\varepsilon_z = 0$	5.1527	4.4107	3.9904	3.4012	3.2816
			$\varepsilon_z \neq 0$	5.1516	4.4230	4.0169	3.4310	3.2984
	2	HSDT [30]	$\varepsilon_z = 0$	17.8840	15.4610	14.0120	11.5350	11.0220
		Present	$\varepsilon_z = 0$	17.8812	15.4588	14.0100	11.5431	11.0240
			$\varepsilon_z \neq 0$	17.8900	15.5052	14.0978	11.6348	11.0785
	3	HSDT [30]	$\varepsilon_z = 0$	34.2250	29.8490	27.1080	21.6990	20.7530
		Present	$\varepsilon_z = 0$	34.2097	29.8382	27.0979	21.7158	20.5561
			$\varepsilon_z \neq 0$	34.2975	29.9670	27.2813	21.8884	20.6748
20	1	HSDT [30]	$\varepsilon_z = 0$	5.4600	4.6510	4.2050	3.6480	3.5390
		Present	$\varepsilon_z = 0$	5.4603	4.6511	4.2051	3.6485	3.5390
			$\varepsilon_z \neq 0$	5.4602	4.6657	4.2351	3.6835	3.5595
	2	HSDT [30]	$\varepsilon_z = 0$	21.5730	18.3960	16.6340	14.3730	13.9260
		Present	$\varepsilon_z = 0$	21.5732	18.3962	16.6344	14.3746	13.9263
			$\varepsilon_z \neq 0$	21.5710	18.4520	16.7511	14.5094	14.0043
	3	HSDT [30]	$\varepsilon_z = 0$	47.5940	40.6530	36.7690	31.5720	30.5340
		Present	$\varepsilon_z = 0$	47.5930	40.6526	36.7679	31.5780	30.5369
			$\varepsilon_z \neq 0$	47.5841	40.7709	37.0192	31.8649	30.7005

Again, the results obtained by the present model, when the thickness- stretching is neglected, correlate closely with these obtained by the HSDT solution [30]. HSDT model under-estimates the frequencies of thick FG beams. This is due to the stretching of de the beam thickness omitted by the HSDT formulation in the thick FG-beams case. It is emphasised that in the HSDT [30] formulation, the unknowns number is greater than this provided by the present model.

Dimensionless frequency variation versus material parameter for an (L/h=5) with and without taking a count of the thickness stretching is plotted in figure 11.a. The plot showed that increasing (p) leads to a decrease of the frequencies. The highest frequency is achieved for (p=0, completely ceramic beam), and the lowest for (p $\rightarrow\infty$, completely metal beam). This can be explained by the fact that the increase in (p) leads to an increase in the amount of ceramic in the mixture, which is replaced by the metal, and leads to the beam Young's modulus decrease and makes it more flexible. The offset between both curves shows the thickness stretching impact. It is seen that the frequencies are under-estimated when thickness stretching is omitted. The impact of the slenderness ratio (L/h) on the frequencies is shown in figure 11.b. It is seen that an increase (L/h) leads to an increase of frequencies.

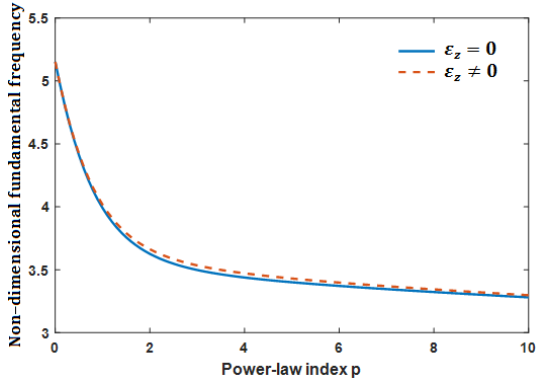

(a)

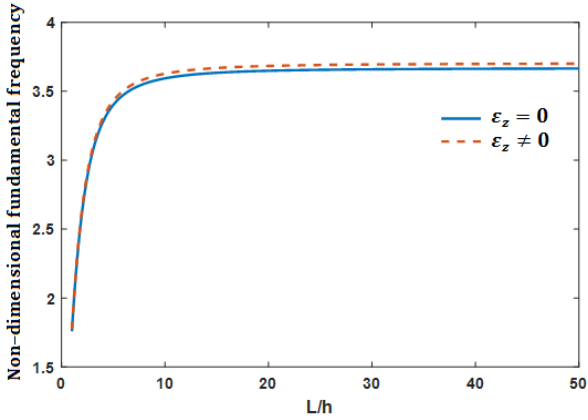

(b)

Figure 11: Effect of (a) the material parameter, (b) beam slenderness, on the dimensionless fundamental frequency of the S-S FG-beam.

Conclusions

In this paper, a refined beam theory is performed for bending vibratory analysis of the thick FG beams, taking into consideration thickness-stretching. The transverse displacement is assumed to be the sum of three components, bending, shear and stretching of the thickness. This leads to reducing the unknown's number of parameters, therefore the number of governing equations. According to a mixing law, the FG beam effective material characteristics are supposed to change continuously along the thickness direction depending on the volume proportion of the constituents. Governing equations are obtained from Hamilton's principle and solved by using Navier-solutions.

Both analytical and numerical results obtained in this article agree with those obtained using other theories with more unknown parameters. Sensitivity analysis has been performed for the thickness-stretching, the material parameter and the beam-slenderness. For this investigation, the shortest beams exhibit the greatest thickness-stretching impact and it needs to be taken into consideration in more physically realistic simulations. Both

geometry and material parameters affect the vibrational responses of the FG beams. Finally, it is observed that the proposed higher order shear and normal deformation theory is not only accurate but also provides an elegant and easily implementable approach for simulating bending and vibration behaviors of FGM beams, of relevance for example in spacecraft thermo-structural design. The formulation lends it self particularly well to finite element simulations and also other numerical methods employing symbolic computation for beam bending problems, which will be considered in the near future. Further applications of our refined FG beam are planned in another contribution to consolidate our approach.

References

1. M Koizumi. FGM activities in Japan, Compos. Part B Eng. 1997; 28: 1–4.
2. JS Moita, AL Araújo, V Franco Correia, CM Mota Soares. Mechanical and thermal buckling of functionally graded axisymmetric shells. Compos. Struct. 2021; 261.
3. F Moleiro, JFA Madeira, E Carrera, JN Reddy. Design optimization of functionally graded plates under thermo-mechanical loadings to minimize stress, deformation and mass, Compos. Struct. 2020; 245.
4. U Gul, M Aydogdu, F Karacam. Dynamics of a functionally graded Timoshenko beam considering new spectrums, Compos. Struct. 2019; 207.
5. XF Li. A unified approach for analyzing static and dynamic behaviors of functionally graded Timoshenko and Euler–Bernoulli beams. J Sound Vib. 2008; 318: 1210–1229.
6. MA Benatta, I Mechab, A Tounsi, EA Adda Bedia. Static analysis of functionally graded short beams including warping and shear deformation effects. Comput Mater Sci. 2008; 44: 765–773.
7. Ben-Oumrane S, Abedlouahed T, Ismail M, Mohamed Bachir B, Mustapha M, et al. A theoretical analysis of flexional bending of Al/Al2O3 S-FGM thick beams. Comput. Mater. Sci. 2009; 44: 1344–1350.

8. SA Sina, HM Navazi, H Haddadpour. An analytical method for free vibration analysis of functionally graded beams. Mater Des. 2009; 30: 741–747.
9. M Şimşek. Static analysis of a functionally graded beam under a uniformly distributed load by Ritz method. Int J Eng Appl Sci. 2009; 1: 1–11.
10. Ghayesh HM. Vibration analysis of shear-deformable AFG imperfect beams. Compos. Struct. 2018; 200: 910–920.
11. R Menaa, A Tounsi, F Mouaici, I Mechab, M Zidi, et al. Analytical solutions for static shear correction factor of functionally graded rectangular beams. Mech Advan Mater Struct. 2012; 19: 641–652.
12. H Yaghoobi, P Yaghoobi. Buckling analysis of sandwich plates with FGM face sheets resting on elastic foundation with various boundary conditions: an analytical approach. Meccanica. 2013; 48: 2019–2035.
13. E Feldman, J Aboudi. Buckling analysis of functionally graded plates subjected to uniaxial loading. Compos Struct. 1997; 38: 29–36.
14. S Abrate. Functionally graded plates behave like homogeneous plates. Composites Part B. 2008; 39: 151–158.
15. M Mahdavian. Buckling analysis of simply-supported functionally graded rectangular plates under non-uniform in-plane compressive loading. J Solid Mech. 2009; 1: 213–225.
16. M Mohammadi, AR Saidi, E Jomehzadeh. Levy solution for buckling analysis of functionally graded rectangular plates. Appl Compos Mater. 2010; 17: 81–93.
17. L Della Croce, P Venini. Finite elements for functionally graded Reissner– Mindlin plates. Comput Meth Appl Mech Eng. 2004; 193: 705–725.
18. J Yang, KM Liew, S Kitipornchai. Second-order statistics of the elastic buckling of functionally graded rectangular plates. Compos Sci Technol. 2005; 65: 1165–1175.
19. X Zhao, YY Lee, KM Liew. Mechanical and thermal buckling analysis of functionally graded plates. Compos Struct. 2009; 90: 161–171.
20. CT Loy, KY Lam, JN Reddy. Vibration of functionally graded cylindrical shells. International Journal of Mechanical Sciences. 1999; 41: 309-324.

21. SC Pradhan, CT Loy, KY Lam, JN Reddy. Vibration characteristics of functionally graded cylindrical shells under various boundary conditions. Applied Acoustics. 2000; 61: 111-129.
22. M Strozzi, F Pellicano. Nonlinear vibrations of functionally graded cylindrical shells. Thin-Walled Structures. 2013; 67: 63-77.
23. F Moleiro, VMF Correia, AL Araújo, CMM Soares, AJM Ferreira, et al. Deformations and stresses of multilayered plates with embedded functionally graded material layers using a layerwise mixed model. Compos. Part B Eng. 2019; 156.
24. HT Thai, TP Vo. Bending and free vibration of functionally graded beams using various higher-order shear deformation beam theories. Int. J. Mech. Sci. 2012; 62.
25. F Ebrahimi, A Jafari. A Higher-Order Thermomechanical Vibration Analysis of Temperature-Dependent FGM Beams with Porosities, J. Eng. (United Kingdom). 2016; 2016.
26. M Aydogdu, V Taskin. Free vibration analysis of functionally graded beams with simply supported edges. Materials & Design. 2007; 28: 1651-1656.
27. Şimşek M. Buckling of Timoshenko beams composed of two-dimensional functionally graded material (2D-FGM) having different boundary conditions. Compos. Struct. 2016; 149.
28. R Patil, S Joladarashi, R Kadoli. Studies on free and forced vibration of functionally graded back plate with brake insulator of a disc brake system. Arch. Appl. Mech. 2020; 90.
29. Z Zhong, T Yu. Analytical solution of a cantilever functionally graded beam. Compos. Sci. Technol. 2007; 67.
30. LO Larbi, A Kaci, MSA Houari, A Tounsi. An efficient shear deformation beam theory based on neutral surface position for bending and free vibration of functionally graded beams. Mech. Based Des. Struct. Mach. 2013; 41.
31. LO Larbi, L Hadji, MAA Meziane, EAA Bedia. An analytical solution for free vibration of functionally graded beam using a simple first-order shear deformation theory. Wind Struct. An Int. J. 2018; 27.

32. M Bouremana, MSA Houari, A Tounsi, A Kaci, EAA Bedia. A new first shear deformation beam theory based on neutral surface position for functionally graded beams. Steel Compos. Struct. 2013; 15.
33. A Fekrar, MSA Houari, A Tounsi, SR Mahmoud. A new five-unknown refined theory based on neutral surface position for bending analysis of exponential graded plates. Meccanica. 2014; 49.
34. AI Osofero, TP Vo, TK Nguyen, J Lee. Analytical solution for vibration and buckling of functionally graded sandwich beams using various quasi-3D theories. J. Sandw. Struct. Mater. 2016; 18.
35. M Meradjah, A Kaci, MSA Houari, A Tounsi, SR Mahmoud. A new higher order shear and normal deformation theory for functionally graded beams, Steel Compos. Struct. 2015; 18.
36. GN Praveen, JN Reddy. Nonlinear transient thermoelastic analysis of functionally graded ceramic-metal plates. Int. J. Solids Struct. 1998; 35.
37. PP Minh, DT Manh, ND Duc. Free vibration of cracked FGM plates with variable thickness resting on elastic foundations. Thin-Walled Struct. 2021; 161.
38. F Tornabene. Free vibration analysis of functionally graded conical, cylindrical shell and annular plate structures with a four-parameter power-law distribution, Comput. Methods Appl. Mech. Eng. 2009; 198.
39. XF Li, BL Wang, JC Han. A higher-order theory for static and dynamic analyses of functionally graded beams. Arch. Appl. Mech. 2010; 80.

APPENDIX A

$$(\mathcal{A}:\mathcal{B}:\mathcal{D}:\mathcal{B}_s:\mathcal{D}_s:\mathcal{H}_s) = \int_{-h/2}^{h/2} (1, z, z^2, \not{f}(z), z\not{f}(z), \not{f}(z)^2) E(z)\, bdz$$

$$(\mathcal{X}, \mathcal{Y}, \mathcal{Y}_s, \mathcal{Z}) = \int_{-h/2}^{h/2} \left(\nu, \nu z, \nu \not{f}(z), \frac{d\not{g}(z)}{dz}\right) \frac{d\not{g}(z)}{dz} E(z)\, bdz$$

$$\mathcal{A}_s = \int_{-h/2}^{h/2} \not{g}(z)^2 \frac{E(z)}{2(1+\nu)} bdz$$

$$(I_0, I_1, I_2) = \int_{-h/2}^{h/2} (1, z, z^2)\rho(z)\, bdz$$

$$(J_0, J_1, J_2) = \int_{-h/2}^{h/2} (\not{g}, \not{f}(z), z\not{f}(z))\rho(z)\, bdz$$

$$(K_0, K_2) = \int_{-h/2}^{h/2} (\not{g}(z)^2, \not{f}(z)^2)\rho(z)\, bdz$$

$$\not{k}_{11} = \mathcal{A}\lambda^2;\ \not{k}_{12} = -\mathcal{B}\lambda^3;\ \not{k}_{23} = \mathcal{D}_{11}^s\lambda^4$$
$$\not{k}_{22} = \mathcal{D}_{11}\lambda^4; \not{k}_{13} = -\mathcal{B}_s\lambda^3; \not{k}_{24} = \mathcal{Y}\lambda^2$$
$$\not{k}_{33} = \mathcal{H}\lambda^4 + \mathcal{A}_s\lambda^2;\ \not{k}_{14} = -\mathcal{X}\lambda;\ \not{k}_{34} = (\mathcal{A}_s + \mathcal{Y}_s)\lambda^2$$
$$\not{k}_{44} = \mathcal{Z} + \mathcal{A}_s\lambda^2$$
$$\not{m}_{11} = I_0\ ;\ \not{m}_{12} = -I_1\lambda\ ;\ \not{m}_{13} = -J_1\lambda$$
$$\not{m}_{22} = I_0 + I_2\lambda^2;\ \not{m}_{23} = I_0 + J_2\lambda^2\ ;\ \not{m}_{24} = J_0$$
$$\not{m}_{33} = I_0 + K_2\lambda^2\ ;\ \not{m}_{34} = J_0\ ;\ \not{m}_{44} = K_0$$